FINAL REPORT

Project Title: High Redshift QSOs and the X-ray Background
Grant Number: NAG 5 1867
Funding Period: 2/15/93 – 10/31/93
Principal Investigator: Chris Impey
Address: Steward Observatory, University of Arizona, Tucson AZ 85721

Summary: ROSAT pointed observations were made of 9 QSOs from the Large Bright Quasar Survey (LBQS). The LBQS is based on machine measurement of objective prism plates taken with the UK Schmidt Telescope. Software has been used to select QSOs by both color and by the presence of spectral features and continuum breaks. The probability of detection can be calculated as a function of magnitude, redshift and spectral features, and the completeness of the survey can be accurately estimated. Nine out of 1040 QSOs in the LBQS have $z > 3$. The observations will provide an important data point in the X-ray luminosity function of QSOs at high redshift. The QSOs with $z > 3$ span less than a magnitude in M_B, so can be combined as a homogeneous sample. This analysis is only possible with a sample drawn from a large and complete catalog such as the LBQS.

Four of the 9 QSOs that were observed with the ROSAT PSPC for this proposal were detected, including one of the most luminous X-ray sources ever observed. The April 1992 version of the PROS DETECT package was used to reduce the data. The results have been used to search for evolution of the X-ray properties of QSOs in redshift. The 9 QSOs lie in the range $-28.7 < M_B < -27.8$. When combined with data for 16 QSOs in a similar luminosity range at lower redshift correlations with luminosity and redshift can be separated out. The LBQS sample also yields a new constraint on the contribution of high redshift QSOs to the X-ray background. An initial requirement is knowledge of the X-ray properties (α_{ox}) as a function of redshift. Integration over the evolving luminosity function of the LBQS then gives the QSO contribution to the source counts.

One University of Arizona graduate student, Tim Pickering, was partially supported on this grant. He presented the results of this project at the AAS Meeting in Arlington, Virginia in January 1994. The results are contained in a paper which has been submitted to the Astrophysical Journal.

Attachment: Paper describing results of the research.

ROSAT Observations of $z > 3$ Quasars

T. E. Pickering and C. D. Impey

Steward Observatory, University of Arizona, Tucson, AZ 85721

E-mail: tpickering@as.arizona.edu, cimpey@as.arizona.edu

and

C. B. Foltz

Multiple Mirror Telescope Observatory, University of Arizona, Tucson, AZ 85721

E-mail: cfoltz@as.arizona.edu

Received _____; accepted _____

ABSTRACT

Successful pointed observations using the ROSAT PSPC were made of 7 $z > 3$ optically-selected quasars from the Large Bright Quasar Survey (LBQS). Four detections and three 3σ upper limits resulted. Combining these data with the heterogeneous sample of Avni & Tananbaum (1986) confirms their conclusion that the ratio of X-ray to optical luminosity is correlated with optical luminosity and probably not correlated with redshift. This suggests that X-ray luminosity evolves more slowly than optical luminosity. These results are then used in conjunction with the LBQS database to estimate the contribution to the X-ray background of bright, optically-selected quasars; the result is about 5%.

1. Introduction

X-ray emission seems to be a ubiquitous property of quasars (e.g., Avni & Tananbaum 1986; henceforth AT86). Observations using the *Einstein Observatory* and the *Roentgen Satellite (ROSAT)* have greatly increased our understanding of the X-ray properties of quasars and AGNs in general. However, until recently most of this understanding has been based on AGNs at relatively low redshift ($z \lesssim 1$). For example, the redshift distribution of AGNs in the *Einstein Observatory* Extended Medium Sensitivity Survey (EMSS; Gioia *et al.* 1990) peaks at $z = 0.1$–0.2. The EMSS contains no AGNs or quasars with $z > 3$ and only 4 with $z > 2$ out of a total of 427. The heterogeneous sample of AT86 contains 5 quasars out of 154 with $z > 3$, of which only 2 were detected.

The high sensitivity of the *ROSAT* Position Sensitive Proportional Counter (PSPC) now allows high-redshift quasars to be detected more efficiently than with previous instruments. The AGNs in the Shanks *et al.* (1991) sample have a significantly higher median redshift than the EMSS: 1.5 as opposed to 0.4. This greater sensitivity makes observing high-redshift samples feasible with moderate exposure times. The sample described in this paper consists of seven $z > 3$ quasars contained in the Large Bright Quasar Survey (LBQS) (Foltz *et al.* 1987, 1989; Hewett *et al.* 1993) that were observed with the *ROSAT* PSPC. Though this LBQS sample is small, it is a significant fraction of the number of optically-selected quasars observed in the soft X-ray band in this redshift range. This sample combined with other lower redshift samples is large enough and now spans enough of a range in redshift to discern any strong correlation, if one exists, between redshift and the ratio of X-ray and optical luminosities. This ratio is traditionally parameterized as the optical to X-ray spectral index, α_{ox}. No obvious correlation of α_{ox} with redshift was found by AT86, though their Detections and Bounds (DB) analysis couldn't rule one out. On the other hand, a correlation between α_{ox} and $L_{\rm opt}$ was claimed by AT86. This can be

converted into the form $L_x \propto L_{\rm opt}^{0.8\pm0.1}$.

Using an expression for α_{ox} as a function of $L_{\rm opt}$ and z, the X-ray properties of optically-selected AGNs can be predicted and compared with those of samples directly observed in the X-ray band. Predicting X-ray properties using $\alpha_{ox}(z, L_{\rm opt})$ is not as reliable as direct X-ray measurements, but it does provide a convenient and practical way of predicting the X-ray properties of large and homogeneous optical samples such as the LBQS.

2. Observations

The observations reported here were performed using the *ROSAT* PSPC in pointed mode with exposure times of 3300–6600 seconds. A missed pointing caused two objects (0301−0035 and 0302−0019) to be near the edge of the PSPC field where vignetting and blurring are severe; it was deemed impractical to try to derive reliable estimates of flux upper limits for these objects. Furthermore, the spacecraft wobble was turned off during the observations of two of the undetected objects, 1244+1129 and 1209+1524, so that obstruction by detector wires may have affected these observations. The rest of the observations were performed with the wobble on and with the objects on-axis or within 16 arcminutes of the center of the field.

Source count rates were derived from 2 arcminute radius circular areas centered on the position of the sources, a region that should contain $\gtrsim 95\%$ of the flux from the source (Wilkes *et al.* 1992). Background count rates were derived from annular regions centered on the source. The sizes of the latter vary due to the proximity of other sources in the field and, in one case, the proximity of a support rib. For nondetections, a 3σ upper limit for the count rate is derived. While the primary motivation for using a 3σ cutoff is for convenience when comparing with other samples that include 3σ upper limits, it is a conservative cutoff.

The LBQS optical positions are accurate to about ±1.5 arcseconds (Hewett *et al.* 1994) and the X-ray positions of the detections all fall within 15 arcseconds of the optical positions. Accurate *a priori* knowledge of the source position reduces the likelihood of confusing the source with a noise fluctuation. The seven fields observed contain on average less than three $> 3\sigma$ serendipitous detections within 20 arcminutes of the image center so the probability of an unrelated real source occuring within the 15 arcsecond radius error circle is less than 0.1% per image.

Table 1 lists the exposure times, count rates, redshifts, B_J magnitudes, 0.4–2.4 keV broadband fluxes, and monochromatic optical and X-ray rest frame luminosities for the objects in this sample. The broadband fluxes were calculated from the count rates using the most recent available PSPC response matrix and an assumed spectral shape of an absorbed power law, $f_x \propto A(N_{HI})\nu^{\alpha_x}$. The energy index, α_x, was assumed to be -0.5 and the absorption is assumed to be galactic with N_{HI} values derived from the Stark *et al.* (1992) data set. This value of α_x and a cosmology of $H_0 = 50$ km s^{-1} Mpc^{-1} and $q_0 = 0.0$ were used in the calculation of luminosities to compare with those of AT86. The apparent B_J magnitudes were converted to absolute B magnitudes, M_B, in the source frame using k-corrections calculated from the composite spectrum of Francis *et al.* (1991). Although there are sizable uncertainties due to variations between individual quasar spectra, the smaller number of quasars contributing to the composite blueward of Lyman-α, and the presence of Lyman series absorption, the composite spectrum gives a more accurate representation of the average quasar spectrum in the region observed in B at redshifts greater than 3 than a simple power law. None of the redshifts are high enough for Lyman limit absorption to fall into the B band. The monochromatic rest frame luminosities at 2500 Å, $L_{\rm opt}$, are then calculated from M_B using the relation:

$$\log L_{\rm opt} = 20.71 - \alpha_o \log\left(\frac{2500}{4400}\right) - M_B/2.5 \qquad (1)$$

where the assumed optical power law slope, α_o, is -0.5. This value is somewhat steeper than the composite spectrum slope of -0.3 between 2500 Å and 4400 Å. However, the difference is not significant since the scatter in the composite spectrum slope due to variation between individual spectra is about 0.9. The monochromatic rest frame luminosities at 2 keV, L_x, are calculated from the 0.4–2.4 keV broadband fluxes using the relations in Schmidt & Green (1986) with an assumed $\alpha_x = -0.5$.

3. X-ray Luminosity as a Function of Optical Luminosity and Redshift

3.1. Optically-Selected Case

The sample used here to look for functional dependencies of L_x (parameterized in terms of α_{ox}) on $L_{\rm opt}$ and z consists of the data used by AT86 in their analysis plus the data given in this paper. The AT86 dataset consists of X-ray observations of a heterogeneous sample of optically discovered quasars plus X-ray observations of two complete, optically-selected samples: the Bright Quasar Survey (Schmidt & Green 1983, Tananbaum *et al.* 1986) and the Braccesi Faint sample (Marshall *et al.* 1984). The heterogeneous sample of AT86 consists of 53 quasars of which 24 are detections, the Bright Quasar Survey sample consists of 66 quasars with 57 detections, and 35 quasars with 13 detections are contained in the Braccesi Faint sample.

The Detections and Bounds regression method of AT86 was used to perform a regression of α_{ox} on $L_{\rm opt}$ and z where $\alpha_{ox} = (\log L_{\rm opt} - \log L_x)/2.606$. A linear dependence of the mean α_{ox}, $\bar{\alpha}_{ox}(z, L_{\rm opt})$, is assumed with the form:

$$\bar{\alpha}_{ox}(z, L_{\rm opt}) = A_z[\tau(z) - 0.5] + A_{\rm opt}(\log L_{\rm opt} - 30.5) + A \qquad (2)$$

where $\tau(z)$ is the look-back time and A_z and $A_{\rm opt}$ are the linear dependence coefficients.

The subtraction terms are chosen to relate A to be the typical α_{ox} for central values of $\tau(z)$ and $\log L_{\rm opt}$ in the whole sample. This is the same form used by AT86.

The distribution of residuals about this average α_{ox} is assumed to be gaussian or a skew distribution of joined half-gaussians. These half-gaussians are treated as separate right and left sides with widths σ_R and σ_L and are normalized to have the same height. AT86 find a significant amount of skewness in their analysis, but it has little effect on the best-fit functional dependence of the mean on either z or $L_{\rm opt}$. However, in the case for the skew distribution the mean relation for α_{ox} is not the same as the "most probable" relation. This "most probable" relation, the mode of the distribution, is related to the mean by $\bar{\alpha}_{ox} + d$ where

$$d = -\sqrt{\frac{2}{\pi}}(\sigma_R - \sigma_L). \tag{3}$$

The degree of skewness is measured by the parameter R which is is defined to be

$$R = \frac{\sigma_R}{\sigma_L}. \tag{4}$$

The relation for σ in terms of σ_R and σ_L is

$$\sigma^2 = \left(1 - \frac{2}{\pi}\right)(\sigma_L^2 + \sigma_R^2) + \left(\frac{4}{\pi} - 1\right)\sigma_L\sigma_R. \tag{5}$$

Figure 1 shows the DB analysis results assuming gaussian residuals. The effect of adding the LBQS sample to the sample of AT86 is slight. The best fit values and the confidence limits for both cases are not significantly different. Under the different assumptions for q_0 and α_x, $A_z = 0$ is still consistent at the 2σ level and $A_{\rm opt} = 0$ is still rejected at the 2σ level. Therefore, the qualitative results of this work are not strongly affected by the assumed cosmology or X-ray spectral shape. The best-fit parameters with the LBQS data included and assuming a skew distribution are $A = 1.53$, $A_z = 0.00$, $A_{\rm opt} = 0.11$, $\sigma = 0.21$, and $R = 3.3$ ($q_0 = 0$ and $\alpha_x = \alpha_o = -0.5$). The best-fit parameters assuming gaussian residuals ($R \equiv 1$) are not significantly different. Little or no dependence

of α_{ox} on z is indicated (see Figure 2). Figure 3 shows the data used in the DB analysis and the best-fit mean relation for $\alpha_{ox}(z, L_{\rm opt})$ (solid line) and the best-fit "most probable" relation for a skew distribution of residuals (dashed line). This "most probable" relation corresponds to $L_x \propto L_{\rm opt}^{0.7\pm0.1}$ and implies that for luminosity dependent evolution models L_x evolves more slowly than $L_{\rm opt}$.

3.2. X-ray Selected Case

It has been noted earlier in the literature (e.g. Kriss & Canizares 1985) that α_{ox} distribution functions for X-ray selected samples differ from those for optically-selected samples. To test this hypothesis, an α_{ox} regression analysis was performed on the X-ray selected AGN sample from the EMSS. In this case $\bar{\alpha}_{ox}$ is assumed to be a function of $\tau(z)$ and L_x with the form:

$$\bar{\alpha}_{ox}(z, L_x) = A_z[\tau(z) - 0.5] + A_x(\log L_x - 26.5) + A \qquad (6)$$

where the fitting coefficients and subtraction terms are analogous to those used for the optically-selected sample. As noted above, the relations in Schmidt & Green (1986) are used to calculate X-ray luminosities from the published 0.3–3.5 keV fluxes assuming $q_0 = 0$ and $\alpha_x = -0.5$. A power law slope of $\alpha_o = -0.5$ and the k-corrections for the V band given in AT86 are used to calculate $L_{\rm opt}$ in the rest frame from the published V magnitudes. The results from the analysis on the EMSS sample are $A = 1.56$, $A_z = 0.79$, $A_x = -0.17$, $\sigma = 0.13$, and $R = 1.1$. The 2σ and 3σ confidence levels for A_z and A_x are shown in Figure 4. The best fit values for these parameters corresponds to $\log L_x \propto 1.8 \log L_{\rm opt} - 3.7\tau(z)$. This is significantly different from and more complicated than the form of $L_x(L_{\rm opt}, z)$ found for the optically-selected sample. Using the relations in Kriss & Canizares (1985) it can be shown that this relation also implies that L_x may evolve more slowly than $L_{\rm opt}$.

Unlike the results from the optically-selected sample, the case of no dependence on z ($A_z = 0$) is excluded at a high confidence level by the results from the EMSS sample. The result for the dependence on $L_{\rm opt}$ from the optically-selected sample corresponds to $A_x = 0.1$ which also differs at a high confidence level from the value derived for the EMSS sample. These results give tighter constraints than those derived by Kriss & Canizares (1985) due to the larger sample size. The discrepancy between the optically and X-ray selected cases may be due to the X-ray selected samples containing a greater fraction of radio-loud quasars. Radio-loud quasars may have an extra component of X-ray emission that is produced by the same process that produces the radio emission (Worrall *et al.* 1987). This correlation of X-ray luminosity with radio emission will cause radio-loud quasars to be preferentially included in X-ray selected samples. X-ray emission in radio-loud quasars may evolve differently than in radio-quiet ones which may explain the differing X-ray evolution of X-ray and optically-selected samples.

3.3. Other High Redshift Samples

The high-z sample of Bechtold *et al.* (1994) consists of 12 detected quasars plus one non-detection in the redshift range from 2.8 to 4.1. This sample is divided into 6 radio-loud quasars and 7 that are radio-quiet. Radio-selected, radio-loud quasars typically have radio emission that is 1000 times stronger than the radio emission of the great majority of optically-selected quasars. The high-z LBQS sample we observed is largely radio-quiet. One quasar in our sample, 0256−0000, is observed to be radio-loud with $\log L_r = 26.43$ (W Hz^{-1}) and 3 others (2231−0015, 0041−2638, and 1209+1524) are observed to be radio-quiet with $\log L_r \simeq 25$ (W Hz^{-1}) or less (Hooper *et al.* 1994; $H_0 = 50$ km s^{-1} Mpc^{-1}, $q_0 = 0.5$). Since only 10% of the LBQS is radio-loud at any redshift (Hooper *et al.* 1994), it is likely that none of the quasars in the rest of our sample are radio-loud.

The LBQS sample and that of Bechtold *et al.* (1994) have similar mean values of z and $L_{\rm opt}$: $\langle z \rangle = 3.2$, $\log(\langle L_{\rm opt} \rangle) = 32.7$ for the LBQS sample and $\langle z \rangle = 3.3$, $\log(\langle L_{\rm opt} \rangle) = 33.0$ for the Bechtold *et al.* sample ($H_0 = 50$ km s^{-1} Mpc^{-1}, $q_0 = 0.0$, $\alpha_x = -0.5$). The predicted $\bar{\alpha}_{ox}(L_{\rm opt})$ for the optically selected case is 1.64 for $\log L_{\rm opt} = 33$. Figure 5 shows the α_{ox} distributions for the LBQS and Bechtold *et al.* (1994) radio-quiet samples. Applying the Kolmogorov-Smirnov (K-S) test to only the detections in both samples shows that they differ at the 93% confidence level. If the limits in both samples are treated as detections, then the K-S test shows a difference at the 94% confidence level. Given the small number of data points in the samples and the fact that the Bechtold *et al.* sample extends to higher $L_{\rm opt}$ than the LBQS sample, these confidence levels should be viewed with caution and don't show a clear discrepancy between the radio-quiet samples.

The radio-quiet quasars in the LBQS and Bechtold *et al.* samples are very clearly more X-ray quiet than the radio-loud quasars in these samples (see Figure 6). If only the detected radio-quiet quasars are considered, then the radio-loud and radio-quiet α_{ox} distributions differ at the 99.9% confidence level according to the K-S test. If the limits are treated as detections, then the K-S test shows the distributions to differ at the 99.7% level. This is consistent with the notion that there is an extra component of X-ray luminosity that correlates with radio luminosity. Interestingly, one of the radio-loud quasars in the Bechtold *et al.* sample was also included in the heterogeneous sample of AT86. This points out a caveat in the use of a heterogeneous sample like this in that it may have radio properties different than a homogeneous optically-selected sample.

4. Predicting the X-ray Background Contribution of Bright Optically-Selected Quasars

The LBQS provides a data-base of 1052 optically-selected AGNs with redshifts from 0.2 to 3.4. Using a relation for α_{ox} in terms of $L_{\rm opt}$ and z, X-ray properties for this sample can be predicted from the optical and redshift data. Here the relation used is $\alpha_{ox} = 0.11(\log L_{\rm opt} - 30.5) + 1.36$. This is the "most probable" relation for the best-fit skew distribution to the AT86 plus LBQS optically-selected sample with any z dependence ignored.

The LBQS contribution to the X-ray background (XRB) is estimated by using $\alpha_{ox}(z, L_{\rm opt})$ to determine a most probable value of L_x for each member of the LBQS sample. The predicted L_x data are then used in conjuction with the redshifts and the effective areas (taken from Hewett *et al.* 1993) to create a predicted $\log N(>S) - \log S$ curve. The predicted curve is then integrated to obtain the estimate of the XRB intensity due to LBQS AGNs. Figure 7 shows the LBQS X-ray number counts curve assuming $\alpha_x = \alpha_o = -0.5$. Integrating this curve gives a background contribution of 4.9% for the LBQS AGNs where $I_{\rm XRB} = 5.99$ keV cm^{-2} s^{-1} sr^{-1} keV^{-1} (Boyle *et al.* 1993). This calculated contribution is dependent on the assumed optical and X-ray spectral shapes and varies from 3.4% for $\alpha_x = \alpha_o = -1$ to 6.2% for $\alpha_x = -0.5$, $\alpha_o = 0.0$. Table 2 shows the breakdown of the contribution of LBQS quasars into bins of de-evolved luminosity and redshift along with the lowest luminosity that could be included in the LBQS within each redshift bin. The optical luminosities are de-evolved using a power-law evolution model of the form

$$L_x(z=0) = L_x(1+z)^{-k} \tag{7}$$

where $k = 3.4$ for $z < 2$ and $k = 1.5$ for $z \geq 2$ (Hewett *et al.* 1993). The de-evolved optical luminosities are then converted to broadband 0.3–3.5 keV luminosities using $\alpha_{ox}(L_{\rm opt})$ and $\alpha_x = -0.5$. The X-ray evolution and luminosity functions derived by Maccacaro *et al.* (1991) and Boyle *et al.* (1993) all give background contributions that peak at about $L_x(z=0) = 10^{43}$–10^{44} ergs s^{-1} and drop off sharply at higher luminosities. This is due to

the break in the X-ray luminosity function that is found to occur in this luminosity range. In each of the redshift bins the limiting de-evolved luminosity for inclusion into the LBQS lies above this break. Thus the low contribution to the XRB of the LBQS AGNs may be due to the LBQS mostly sampling AGNs that contribute to the bright end of the X-ray luminosity function.

5. Conclusions

ROSAT PSPC observations of the LBQS AGNs with $z > 3$ have resulted in four detections and three 3σ upper limits. Combining this small sample with previous measurements gives the qualitative results that α_{ox} has little or no dependence on redshift and is less than linearly related to $L_{\rm opt}$ for optically-selected quasars. The dependence on $L_{\rm opt}$ implies an evolutionary rate for L_x less than that for $L_{\rm opt}$. Using the best estimate of $\alpha_{ox}(L_{\rm opt})$ along with optical data from the LBQS gives an X-ray background contribution at 2 keV of 4.9%.

However, performing a regression of $\alpha_{ox}(z, L_x)$ on the X-ray selected EMSS gives very different results than for the optically-selected sample. The results for the optically and X-ray selected cases differ at greater than the 3σ level. α_{ox} for the X-ray selected case is a function of both L_x and z which corresponds to L_x being dependent on $L_{\rm opt}$ and z. The dependency is such that L_x still has a lower evolution rate than $L_{\rm opt}$. Similar results for the Medium Sensitivity Survey (MSS) subset of the EMSS are discussed in Kriss & Canizares (1985). Boyle *et al.* (1993) find that their relation for L_x in terms of $L_{\rm opt}$ using the faint-ends of the optical and X-ray LF is inconsistent with the relation using the bright-ends. This follows from the relation for $L_x(z, L_{\rm opt})$ derived here. As noted in Boyle *et al.* (1993) and Kriss & Canizares (1985) the inconsistency between optically and X-ray selected samples at the bright end is due to the MSS AGNs being the dominant contributors at the X-ray

bright-end. The inconsistency may be due to the X-ray selected sample containing a greater fraction of radio-loud quasars than optically-selected samples.

The *ROSAT* Medium Sensitivity Survey along with very deep pointed observations such as those by Shanks *et al.* (1991) promise to shed greater light on the X-ray properties of AGNs in general. The observations given here show that the PSPC can reach AGNs at high redshifts with moderate exposure times. Thus more $z > 3$ AGNs should show up in the *ROSAT* Medium Sensitivity Survey.

The authors would like to gratefully thank Jill Bechtold and Fabrizio Fiore for pointing out a bug in the analysis. We also thank Eric Hooper for providing the radio data. This work was supported by NASA grant NAG 5-1867.

REFERENCES

Avni, Y., & Tananbaum, H. 1986 (AT86), ApJ, 305, 83.

Bechtold, J., Elvis, M., Fiore, M., Kuhn, O., Cutri. R. M., McDowell, J. C., Rieke, M., Siemiginowska, A., & Wilkes, B. J. 1994 ApJ, submitted.

Boyle, B. J., Griffiths, R. E., Shanks, T., Stewart, G. C., & Georgantopoulos, I. 1993, MNRAS, 260, 49.

Foltz, C. B., Chaffee, F. H., Hewett, P. C., MacAlpine, G. M., Turnshek, D. A., Weymann, R. J., & Anderson, S. F. 1987, AJ, 94, 1423.

Foltz, C. B., Chaffee, F. H., Hewett, P. C., Weymann, R. J., Anderson, S. F., & MacAlpine, G. M. 1989, AJ, 98, 1959.

Francis, P. J., Hewett, P. C., Foltz, C. B., Chaffee, F. H., Weymann, R. J., & Morris, S. L. 1991, ApJ, 373, 465.

Gioia, I. M., Maccacaro, T., Schild, R. E., Wolter, A., Stocke, J. T., Morris, S. L., & Henry, J. P. 1990, ApJS, 72, 567.

Hewett, P. C., Foltz, C. B., & Chaffee, F. H. 1993, ApJ, 406, L43.

Hewett, P. C., Foltz, C. B., & Chaffee, F. H. 1994, in preparation.

Hooper, E. J., Impey, C. D., Foltz, C. B., & Hewett, P. C. 1994, ApJ, submitted.

Kriss, G. A. & Canizares, C. R. 1985, ApJ, 297, 177.

Maccacaro, T., Gioia, I. M., Wolter, A., Zamorani, G., & Stocke, J. T. 1988, ApJ, 326, 680.

Maccacaro, T., Della Ceca, R., Gioia, I. M., Morris, S. L., Stocke, J. T., & Wolter, A. 1991, ApJ, 374, 117.

Marshall, H. L., Avni, Y., Braccesi, A., Huchra, J. P., Tananbaum, H., Zamorani, G., & Zitelli, V. 1984, ApJ, 283, 50.

Schmidt, M. & Green, R. F. 1983, ApJ, 269, 357.

Schmidt, M. & Green, R. F. 1986, ApJ, 305, 68.

Shanks, T., Georgantopoulos, I., Stewart, G. C., Pounds, K. A., Boyle, B. J., & Griffiths, R. E. 1991, Nature, 353, 315.

Stark, A. A., Gammie, C. F., Wilson, R. W., Bally, J., Linke, R. A., Heiles, C., & Hurwitz, M. 1992, ApJS, 79, 77.

Tananbaum, H., Avni, Y., Green, R. F., Schmidt, M., & Zamorani, G. 1986, ApJ, 305, 57.

Wilkes, B. J., Elvis, M., Fiore, F., McDowell, J. C., Tananbaum, H., & Lawrence, A. 1992, ApJ, 393, L1.

Worrall, D. M., Giommi, P., Tananbaum, H., & Zamorani, G. 1987, ApJ, 313, 596.

This manuscript was prepared with the AAS LaTeX macros v3.0.

FIG. 1 – Results of the DB analysis showing *(a)* the effect of adding the LBQS high-z data set to the full sample used in AT86, *(b)* the effect of changing the assumed value of q_0, and *(c)* the effect of changing the assumed value of α_x on the best estimate and 2σ contour for A_x and $A_{\rm opt}$.

FIG. 2 – α_{ox} data from BQS, BF, HET85, and LBQS datasets plotted versus z. No clear correlation is found by the DB analysis. BQS and BF refer to the Bright Quasar Survey and Braccesi Faint samples, respectively, and HET85 refers to the heterogeneous quasar sample presented in AT86.

FIG. 3 – α_{ox} data from BQS, BF, HET85, and LBQS datasets plotted versus $L_{\rm opt}$. *Solid line:* Best fit mean relation $\bar{\alpha}_{ox} = 0.11(\log L_{\rm opt} - 30.5) + 1.53$. *Dotted line:* Best fit most probable relation $\bar{\alpha}_{ox} + d = 0.11(\log L_{\rm opt} - 30.5) + 1.36$.

FIG. 4 – Best estimate, 2σ, and 3σ contours for A_x and A_x using the EMSS data-base.

FIG. 5 – Cumulative histograms of the α_{ox} distributions for the LBQS and Bechtold *et al.* (1994) radio-quiet samples. The histograms in *(a)* contain only detected quasars while those in *(b)* include the α_{ox} lower limits in the samples as detections.

FIG. 6 – Cumulative histograms of the α_{ox} distributions of the radio loud and radio quiet quasars in the LBQS and Bechtold *et al.* (1994) high redshift samples. The histograms in *(a)* contain only detected quasars while those in *(b)* include the α_{ox} lower limits in the samples as detections.

FIG. 7 – Predicted LBQS X-ray number counts curve. Given values of α_{ox}, α_x, and α_o are used to convert the LBQS optical fluxes to broadband 0.3–3.5 keV X-ray fluxes.

TABLE 1

X-RAY OBSERVATIONS OF A LBQS SAMPLE OF $z > 3$ AGNS

Name	Exposure (s)	Count Rate (10^{-3} s^{-1})	Redshift	B_J	$\log f_x$	$\log L_{\rm opt}$	$\log L_x$
0256−0000	5023	7.4 ± 2.0	3.364	18.22	−13.00	32.869	28.43
0042−2627	5652	5.7 ± 1.5	3.289	18.47	−13.26	32.730	28.14
0101−3025	6633	< 4.6	3.152	18.49	< -13.31	32.612	< 28.04
1244+1129	4177	< 7.0	3.147	18.38	< -13.12	32.651	< 28.23
1209+1524	5668	< 5.1	3.060	18.27	< -13.23	32.602	< 28.08
0041−2638	5652	4.4 ± 1.4	3.053	18.27	−13.37	32.595	27.94
2231−0015	3313	8.3 ± 2.4	3.015	17.53	−12.95	32.849	28.34

NOTE. — Luminosities are monochromatic at 2 keV for L_x and at 2500 Å for $L_{\rm opt}$. The 0.4–2.4 keV X-ray flux, f_x, is in units of ergs cm^{-2} s^{-1}. The monochromatic luminosities L_x and $L_{\rm opt}$ are in units of ergs s^{-1} Hz^{-1}.

TABLE 2

PERCENTAGE CONTRIBUTION TO THE AGN INTENSITY AT 2 KEV FROM DIFFERENT BINS OF LUMINOSITY AND REDSHIFT

$\log L_x(z=0)$	Redshift						
(0.3 – 3.5 keV)	0.35	0.75	1.25	1.75	2.25	2.75	3.25
43–44	0.0	0.0	0.0	0.0	0.0	0.0	0.0
44–45	12.8	21.1	20.8	19.0	17.2	3.5	0.0
45–46	0.0	0.1	1.1	0.8	1.0	1.9	0.8
Limit	43.9	44.3	44.5	44.6	44.7	44.8	45.0

NOTE. — Luminosities in units of ergs s^{-1}. Redshifts denote centers of the respective redshift bins. Limits are the lowest de-evolved X-ray luminosity in each redshift bin that could be contained in the LBQS.

Figure 1

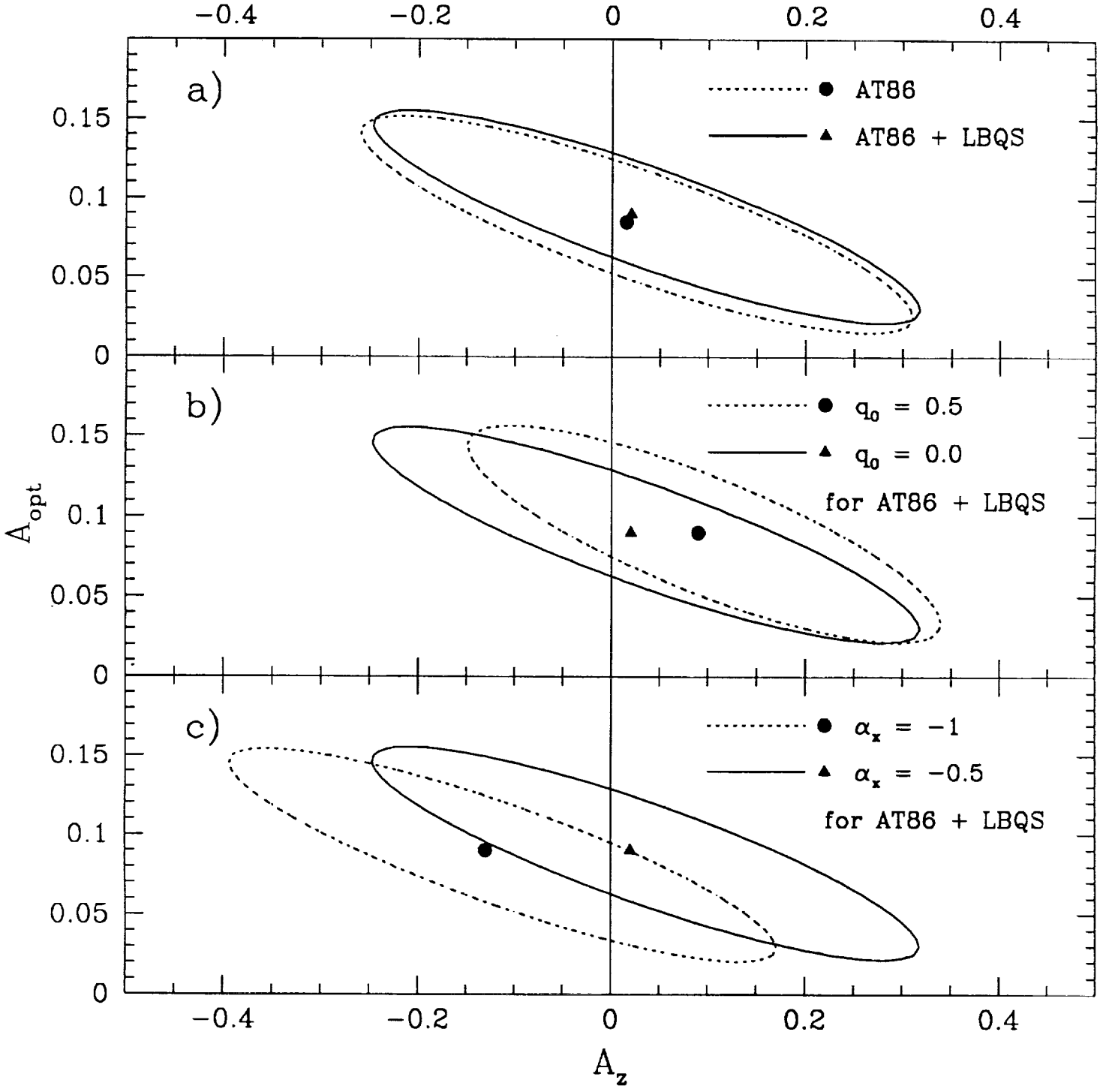
a)
AT86
AT86 + LBQS
b)
q_0 = 0.5
q_0 = 0.0
for AT86 + LBQS
c)
α_x = −1
α_x = −0.5
for AT86 + LBQS
A_{opt}
A_z
−0.4
−0.2
0
0.2
0.4
0.05
0.1
0.15

Figure 2

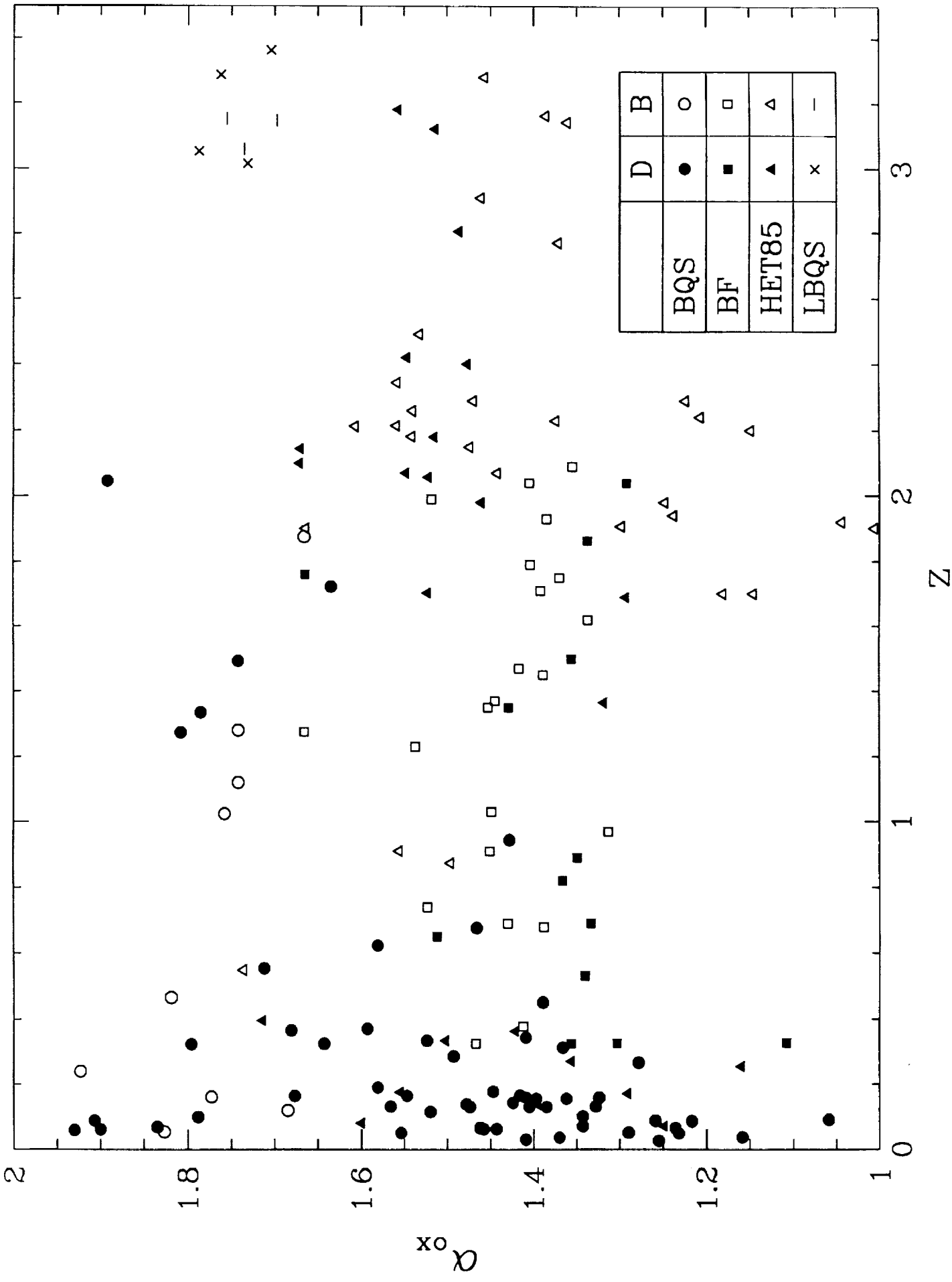

Figure 3

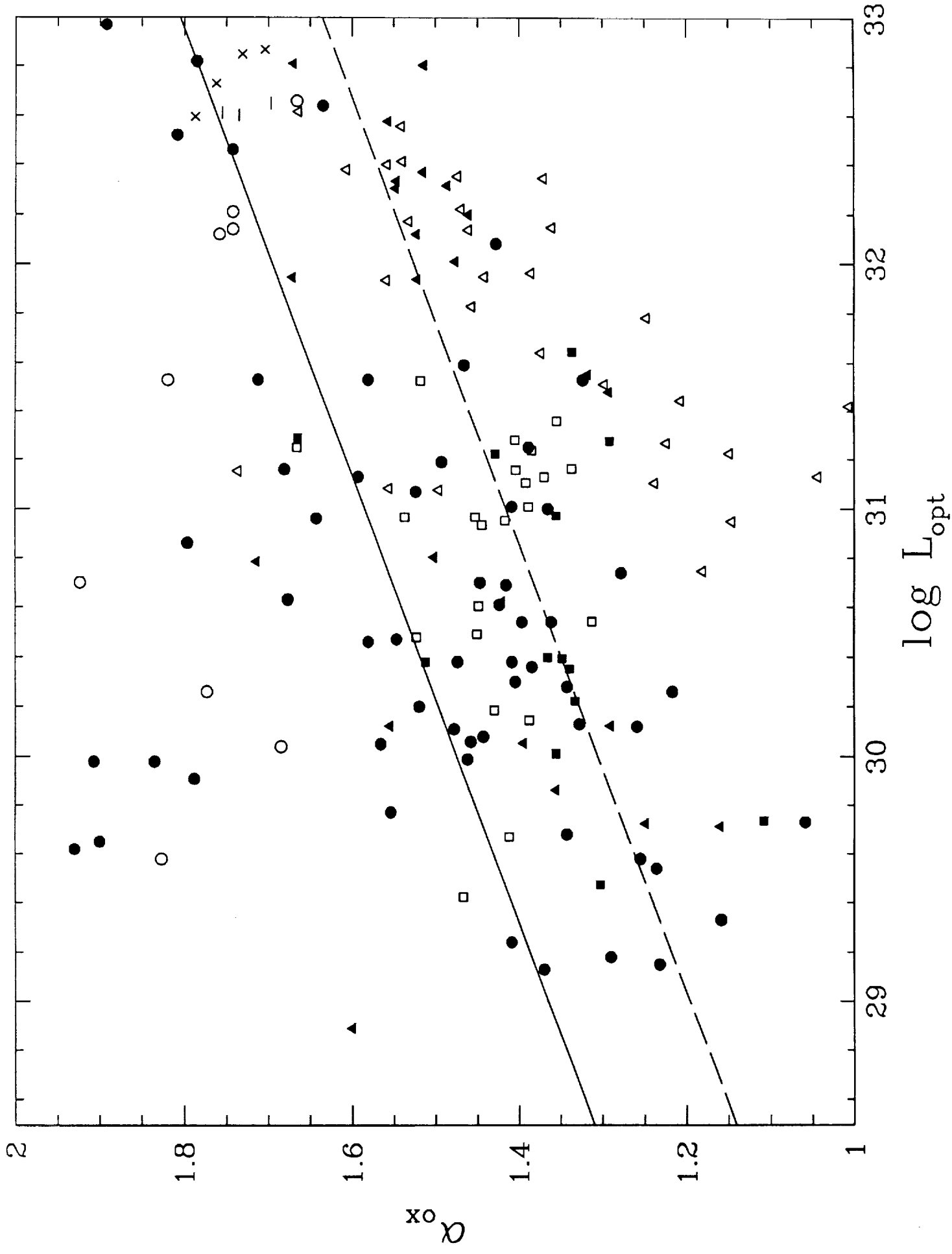

Figure 4

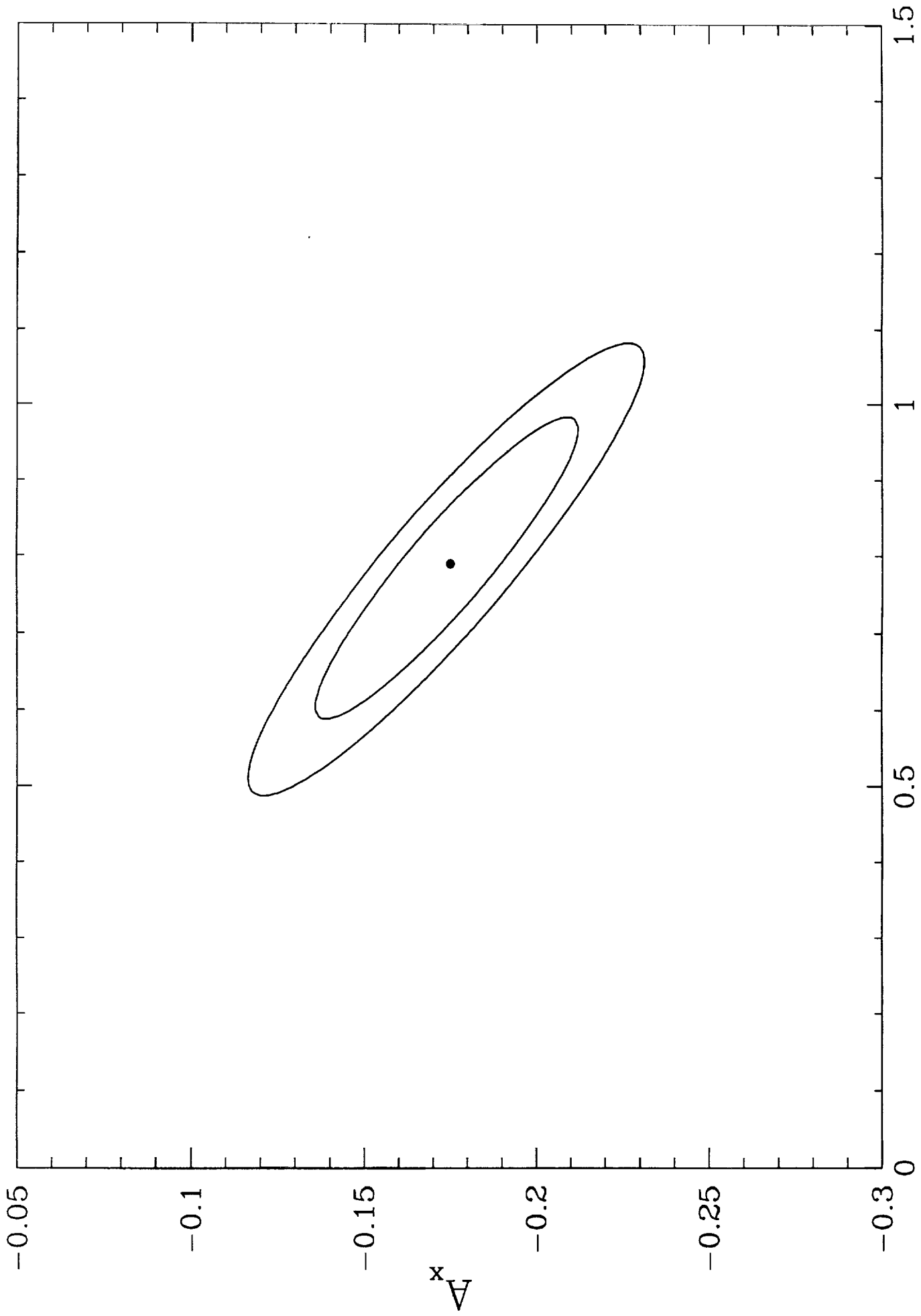

Figure 5

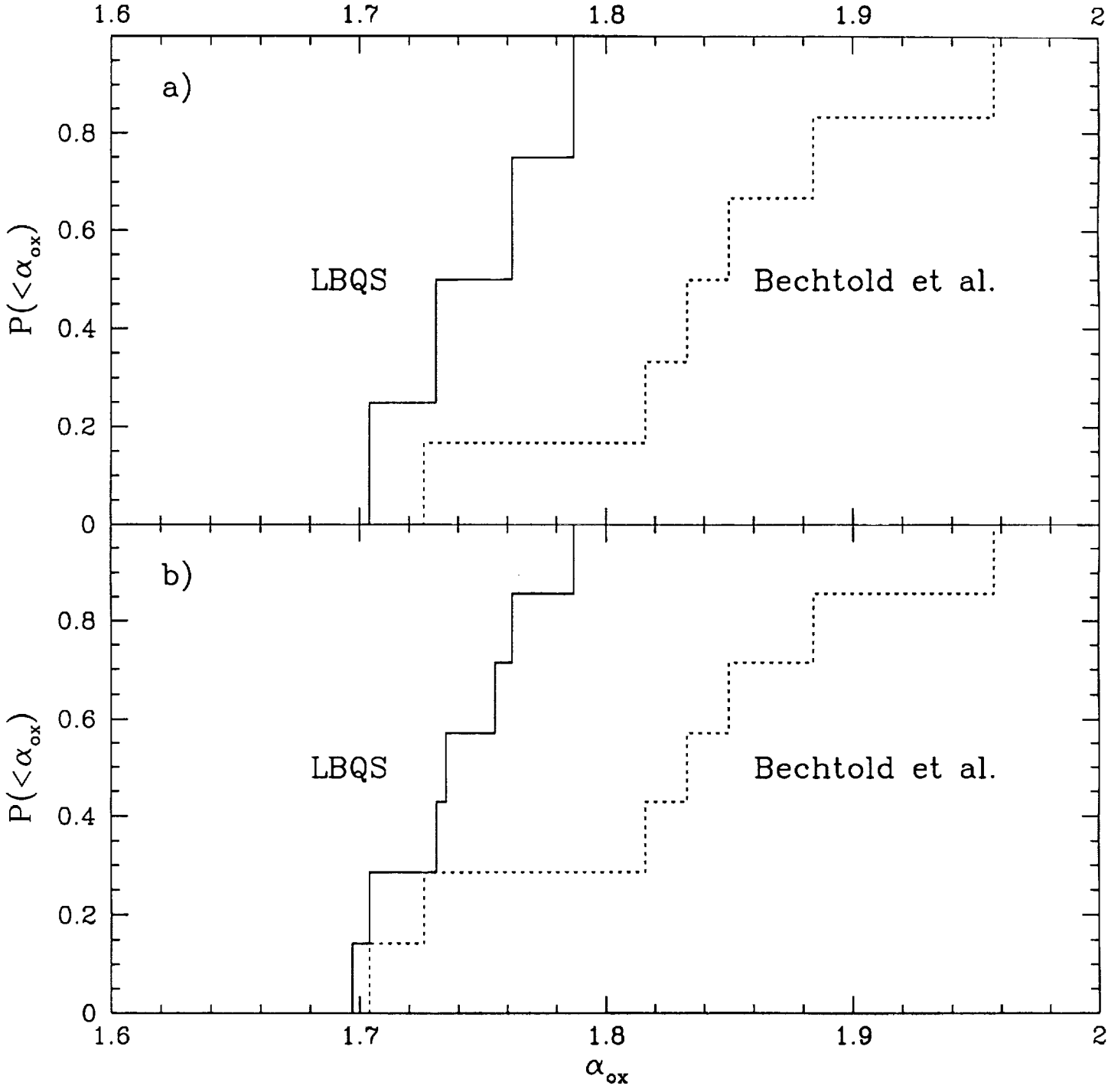
a)
b)
LBQS
Bechtold et al.
LBQS
Bechtold et al.
P(<α_ox)
P(<α_ox)
α_ox
1.6
1.7
1.8
1.9
2
0
0.2
0.4
0.6
0.8

Figure 6

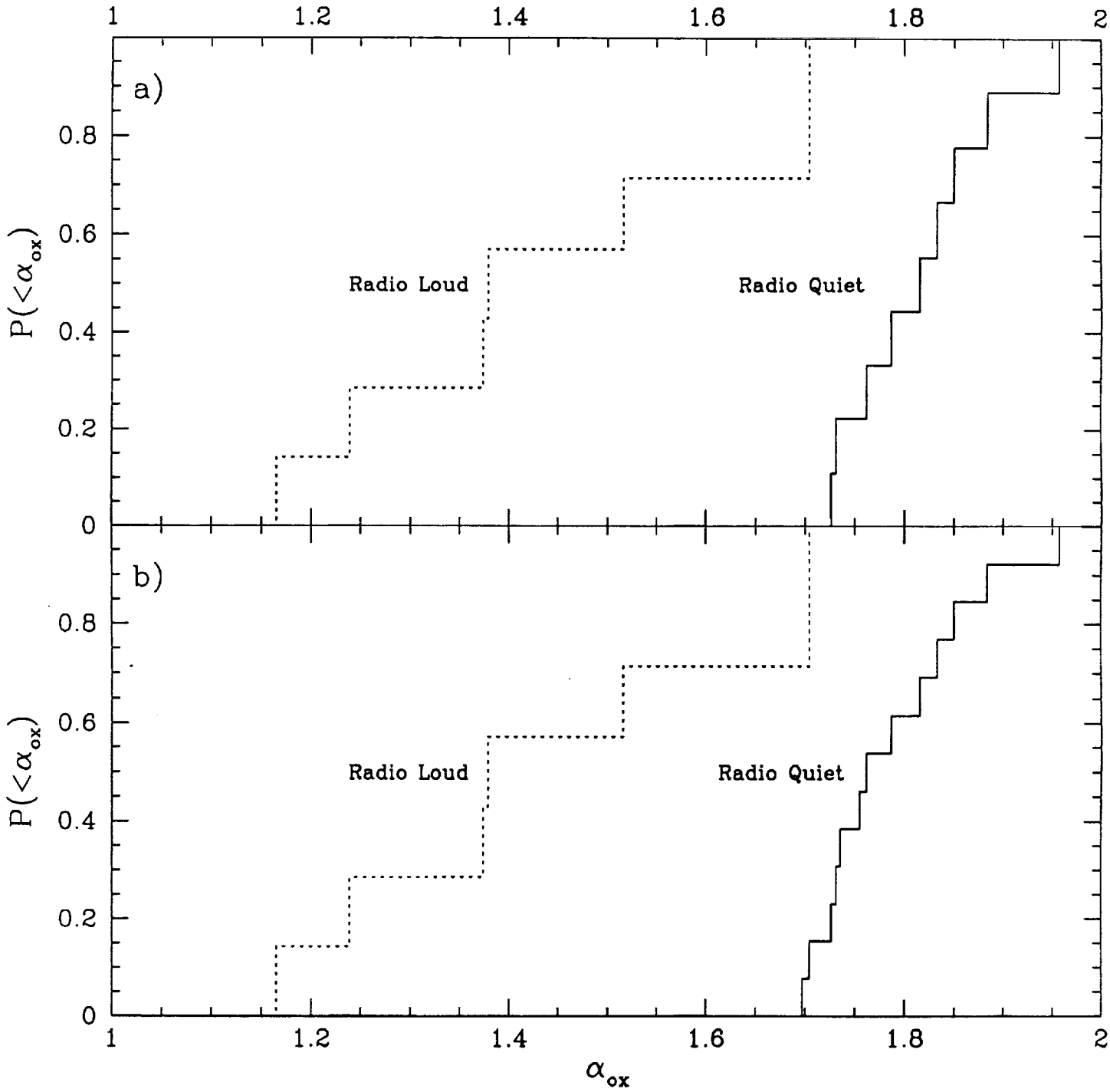
a)
b)
Radio Loud
Radio Quiet
Radio Loud
Radio Quiet
P(<α_ox)
P(<α_ox)
α_ox
1
1.2
1.4
1.6
1.8
2
0
0.2
0.4
0.6
0.8

Figure 7

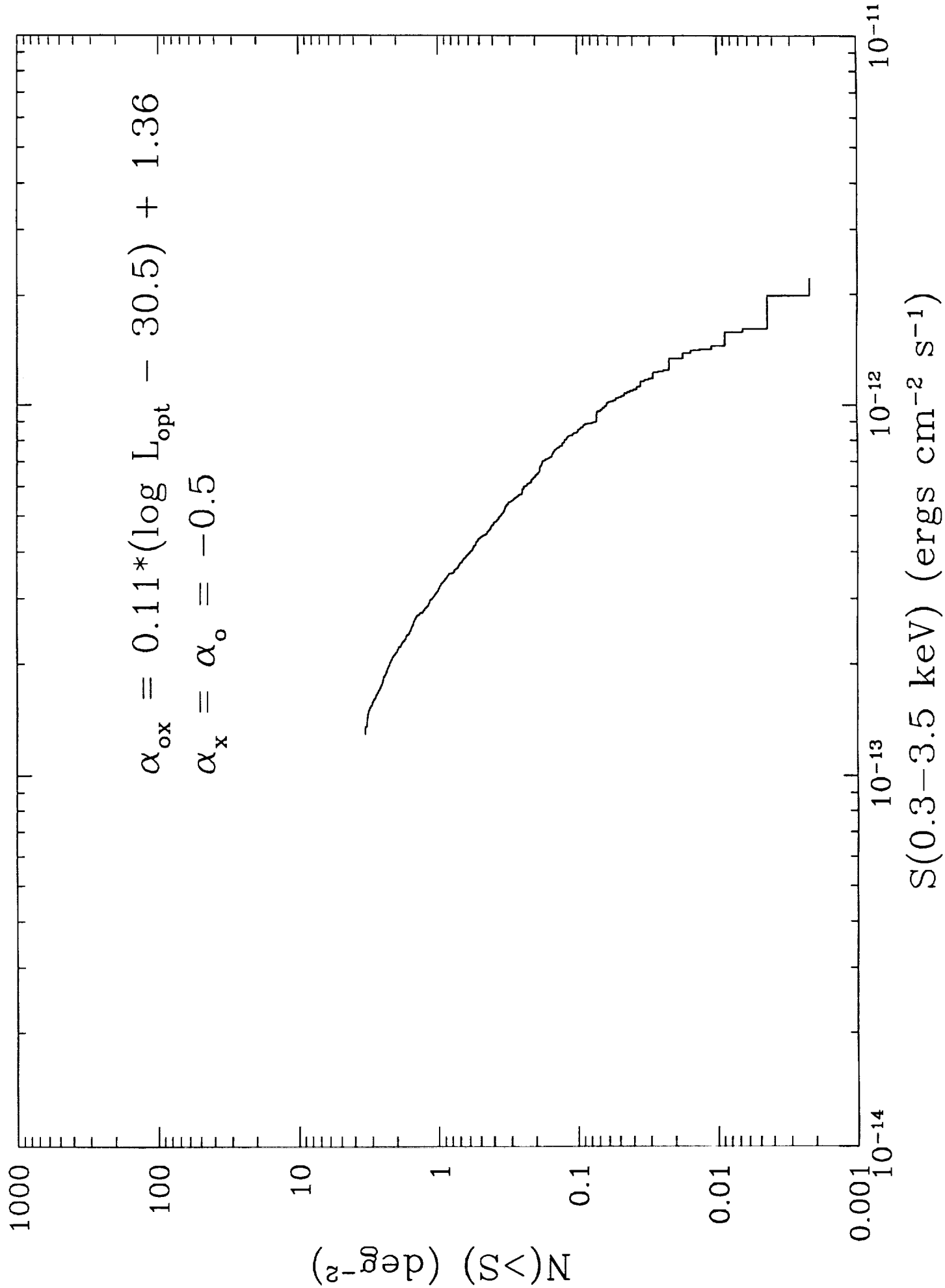
$\alpha_{ox} = 0.11*(\log L_{opt} - 30.5) + 1.36$
$\alpha_x = \alpha_o = -0.5$
N(>S) (deg^{-2})
S(0.3−3.5 keV) (ergs cm^{-2} s^{-1})
1000
100
10
1
0.1
0.01
0.001
10^{-11}
10^{-12}
10^{-13}
10^{-14}